

Supporting Information

Coordination Tuning of Ni/Fe Complexes based Electrocatalysts for Enhanced Oxygen Evolution

Hongbo Zhou, Xuan Hao, Jiexin Guan, Yilin Deng, Zi Wei, Yashu Liu, and Guoxing Zhu*

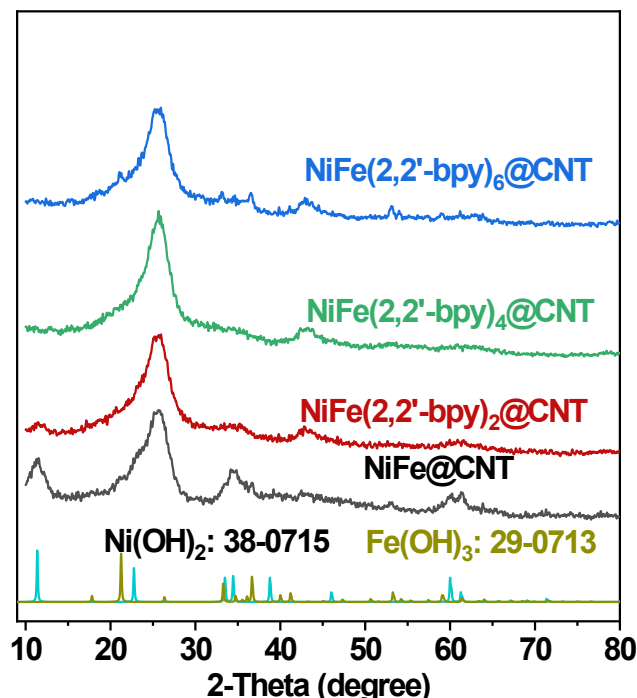


Figure S1 XRD spectra of $\text{NiFe}(2,2'\text{-bpy})_n@\text{CNT}$ after immersion in 1M KOH

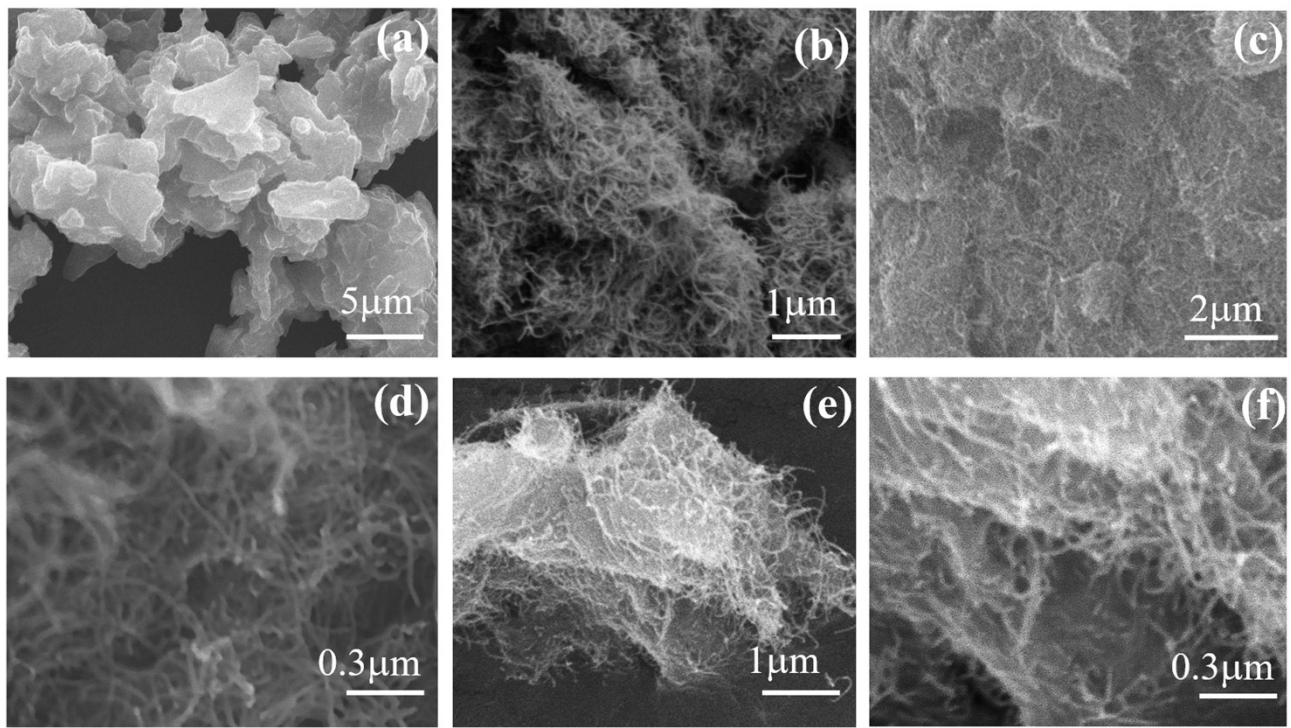


Figure S2 SEM images of pure $\text{NiFe}(2,2'\text{-bpy})_2$ (a), MWCNTs (b) and $\text{NiFe}(2,2'\text{-bpy})_2@\text{CNT}$ (c, d) before OER; the $\text{NiFe}(2,2'\text{-bpy})_2@\text{CNT}$ product after OER (e, f).

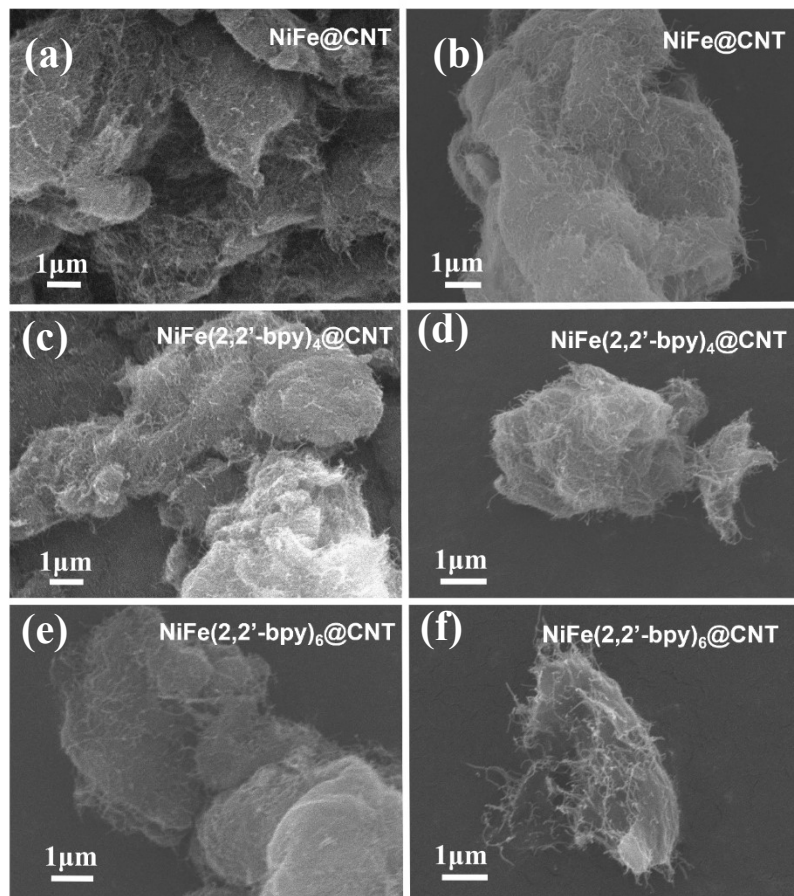


Figure S3 The SEM images of $\text{NiFe}(2,2'\text{-bpy})_n\text{@CNT}$ with $n = 0, 4, 6$ before (a, c, e) and after OER(b, d, f)

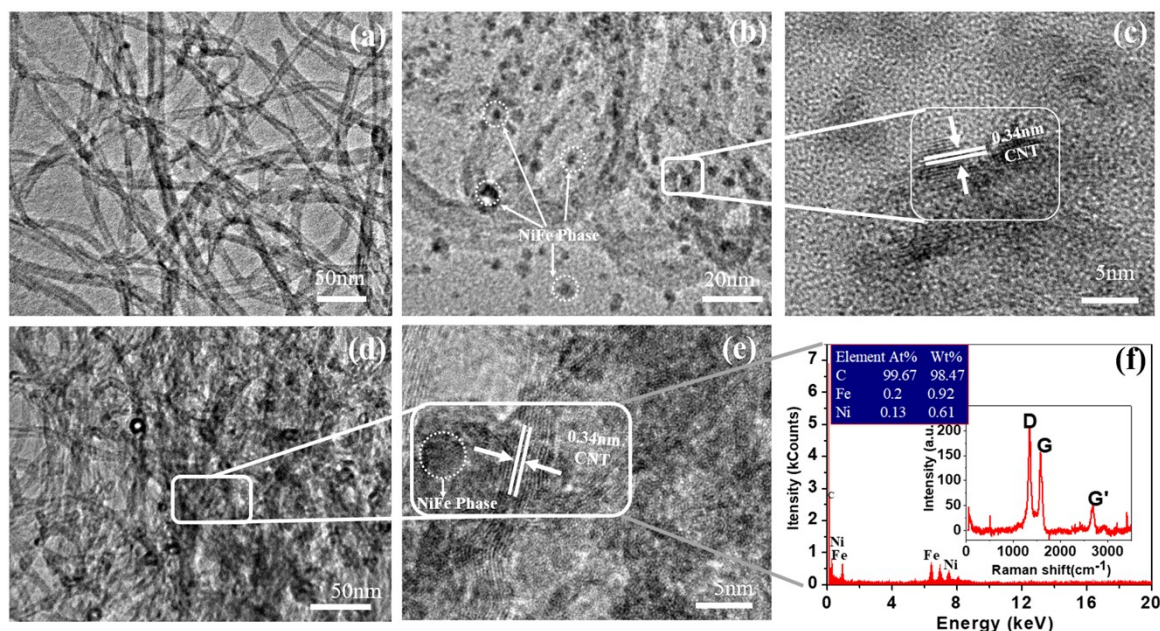


Figure S4 TEM images of pristine MWCNTs (a), NiFe(2,2'-bpy)₂@CNT (b, c), NiFe(2,2'-bpy)₂@CNT (after OER) (d, e), and EDS element analysis of NiFe(2,2'-bpy)₂@CNT (after OER) (f) (Inset: the Raman spectra of the material)

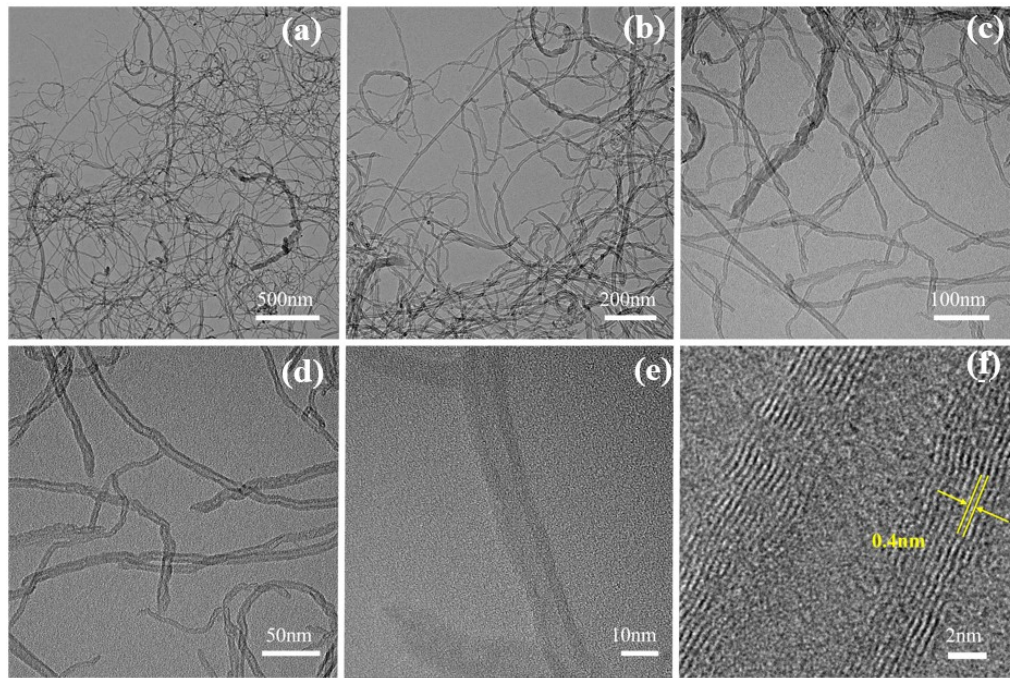
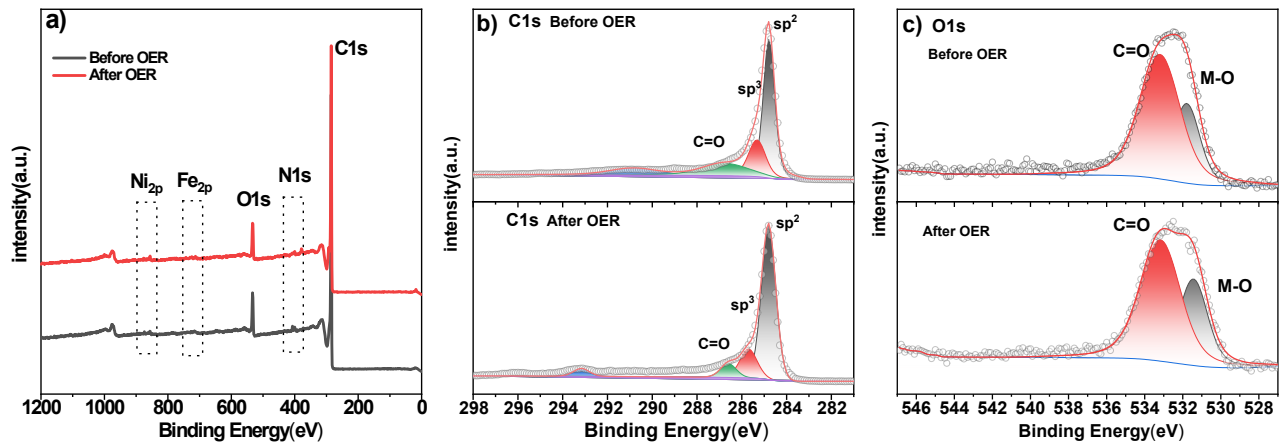


Figure S5 TEM images of NiFe(2,2'-bpy)₂@CNT before OER after long-time ultrasonic processing



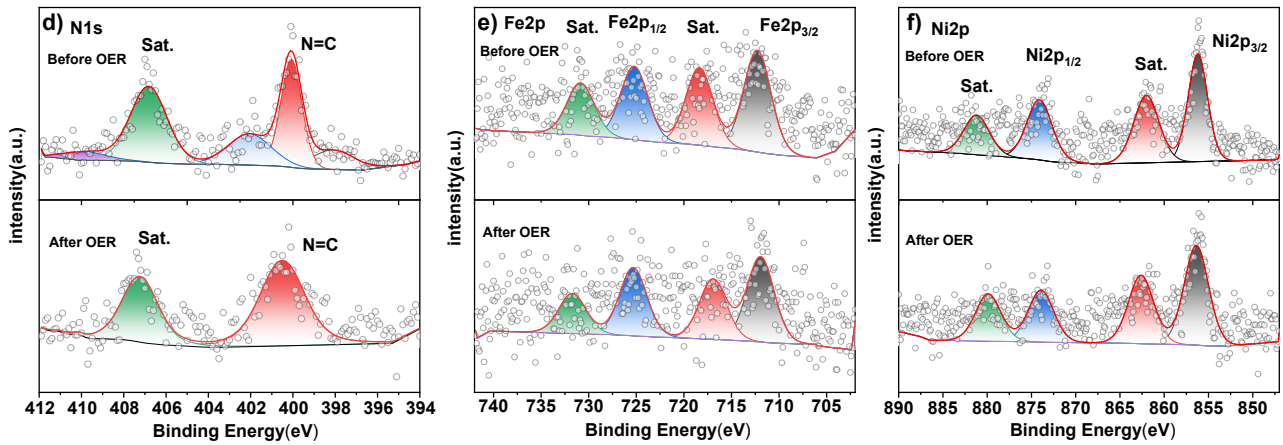


Figure S6. XPS survey spectra (a) and high-resolution XPS spectra of $\text{NiFe}(2,2'\text{-bpy})_n@\text{CNT}$ before after OER (b-f).

Table S1 Ni/Fe content of best-performing sample, $\text{NiFe}(2,2'\text{-bpy})_2@\text{CNT}$ determined from ICP after long-term durability i-t test

Material	Fe(w%)	Ni(w%)
$\text{NiFe}(2,2'\text{-bpy})_2@\text{CNT}$	0.2%	0.1%

Table S2 Metal element content of experimental calculation values with the those obtained from high-resolution XPS fitting

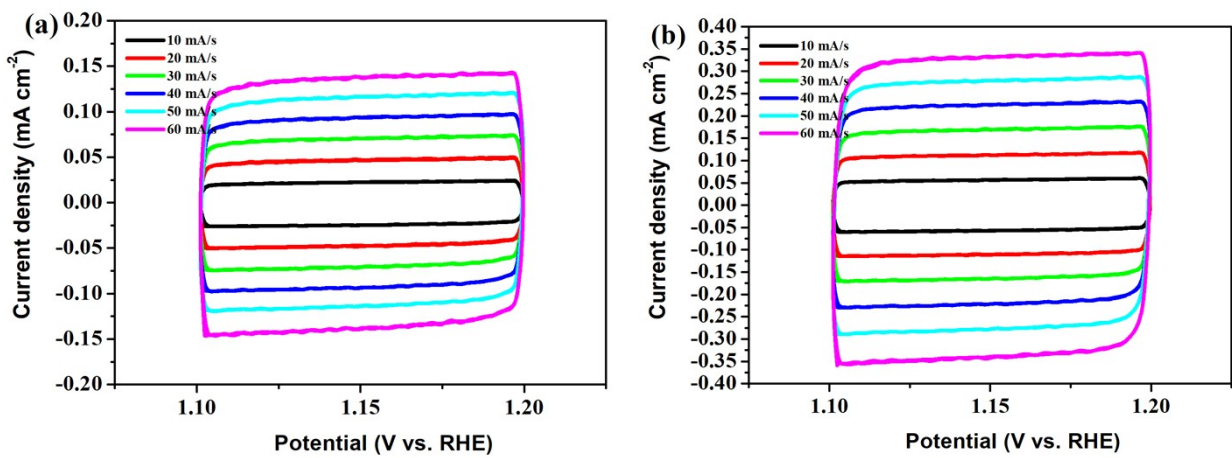
(a) Experimental calculation values

Material	CNT(w%)	Fe(w%)	Ni(w%)
$\text{NiFe}@\text{CNT}$	85.19%	1.19%	1.25%
$\text{NiFe}(2,2'\text{-bpy})@\text{CNT}$	82.44%	1.16%	1.21%
$\text{NiFe}(2,2'\text{-bpy})_2@\text{CNT}$	79.87%	1.12%	1.17%
$\text{NiFe}(2,2'\text{-bpy})_3@\text{CNT}$	77.45%	1.09%	1.14%
$\text{NiFe}(2,2'\text{-bpy})_4@\text{CNT}$	75.18%	1.05%	1.10%
$\text{NiFe}(2,2'\text{-bpy})_5@\text{CNT}$	73.03%	1.02%	1.07%
$\text{NiFe}(2,2'\text{-bpy})_6@\text{CNT}$	71.00%	1.00%	1.04%

(b) Values obtained from high-resolution XPS fitting

Before OER ($\text{NiFe}(2,2'\text{-bpy})_2@\text{CNT}$)							
Name	Peak BE	FWHM eV	Area (P) CPS.eV	Atomic %	Weight %	Atomic %	Weight %
C1s	284.85	0.77	102501.7	51.43	49.01	90.92	86.65
C1s	285.88	2.51	54877.87	27.54	26.25		
C1s	290.46	3.37	23781.04	11.95	11.39		
N1s	400.19	1.52	3230.52	0.99	1.11	1.66	1.86
N1s	407	1.08	2177.49	0.67	0.75		
O1s	531.73	1.52	5690.76	1.06	1.34	6.79	8.61
O1s	532.98	2.89	30744.75	5.73	7.27		

Fe2p	712.27	3.37	2700.95	0.11	0.48		
Fe2p	725.22	3.37	1949.73	0.08	0.35	0.33	1.42
Fe2p	730.86	3.37	1383.27	0.06	0.25		
Fe2p	717.6	3.37	1938.69	0.08	0.34		
Ni2p	856.2	2.57	3512.51	0.1	0.48	0.32	1.48
Ni2p	874.09	3.37	2558.77	0.08	0.36		
Ni2p	862.02	3.37	2872.88	0.09	0.4		
Ni2p	881.2	3.37	1687.62	0.05	0.24		
After OER ($\text{NiFe}(2,2'\text{-bpy})_2@\text{CNT}$)							
Name	Peak BE	FWHM eV	Area (P) CPS.eV	Atomic %	Weight %		
C1s	284.8	0.75	104125.1	64.54	61.15		
C1s	285.7	0.91	23605.7	14.63	13.87	89.19	84.51
C1s	293.16	0.83	5820.62	3.61	3.42		
C1s	286.6	0.83	10334.62	6.41	6.07		
N1s	400.49	3.3	3459.9	1.32	1.45	2.08	2.29
N1s	407.17	2.34	2004.31	0.76	0.84		
O1s	531.25	1.6	6449.29	1.48	1.87	8.05	10.17
O1s	532.92	2.98	28576.65	6.57	8.3		
Fe2p	711.94	3.37	1936.2	0.1	0.42		
Fe2p	725.33	3.37	1551.34	0.08	0.34	0.3	1.26
Fe2p	716.94	3.37	1364.14	0.07	0.3		
Fe2p	731.72	3.37	908.38	0.05	0.2		
Ni2p	856.36	3.26	3839.47	0.14	0.65	0.39	1.76
Ni2p	862.62	3.37	2594.36	0.1	0.44		
Ni2p	873.92	3.37	2066.55	0.08	0.35		
Ni2p	879.88	3.37	1875.38	0.07	0.32		



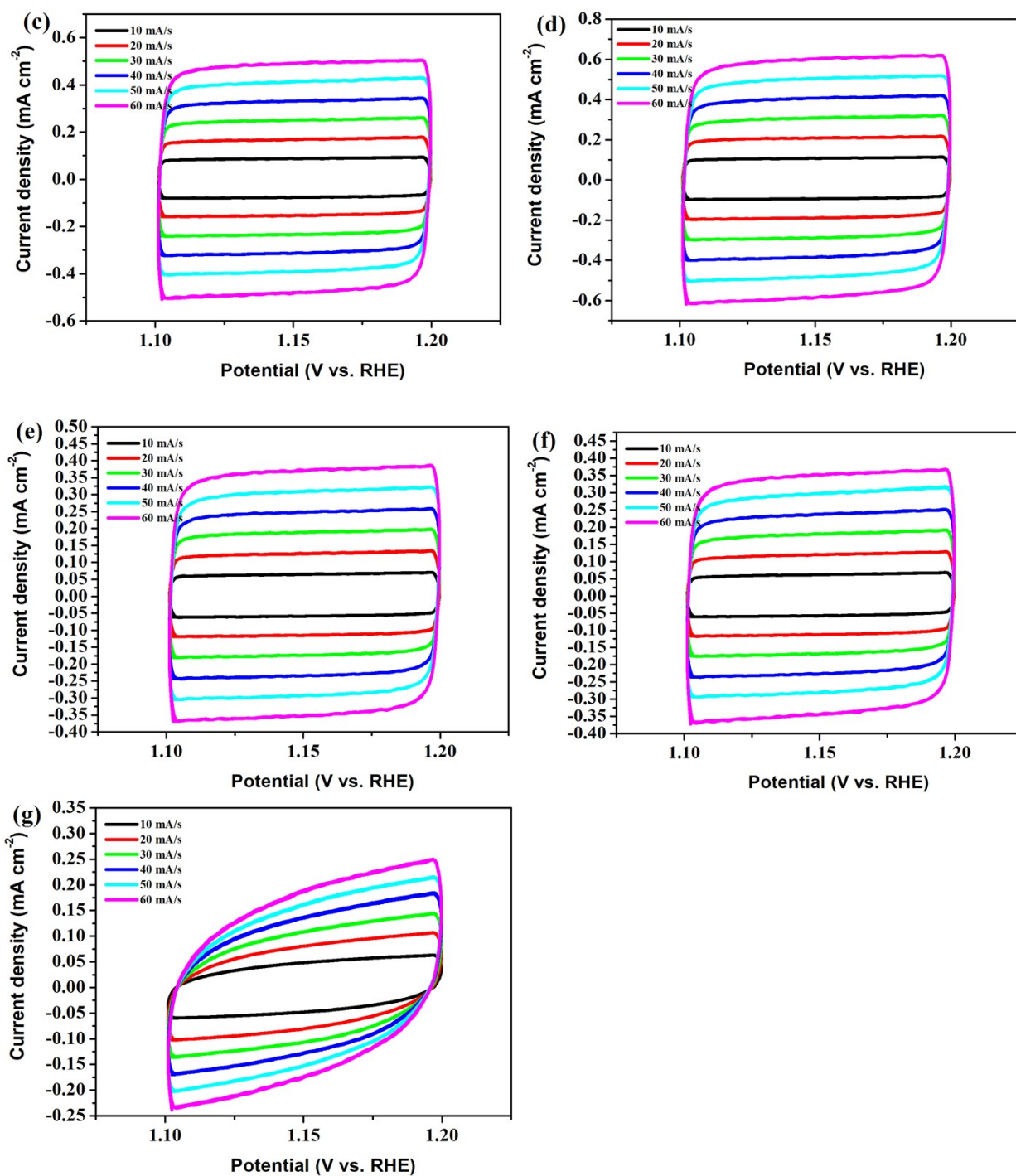


Figure S7 Electrochemical cyclic voltammetry curves of (a) NiFe@CNT, (b) NiFe(2,2'-bpy)@CNT, (c) NiFe(2,2'-bpy)₂@CNT, (d) NiFe(2,2'-bpy)₃@CNT, (e) NiFe(2,2'-bpy)₄@CNT, (f) NiFe(2,2'-bpy)₅@CNT and (g) NiFe(2,2'-bpy)₆@CNT at different scanning rates

Table S3 Values of the double layer capacitance, electrochemical surface area and turnover frequency (TOF) of the catalysts.

Material	Double layered capacitance (C_{dl}) ($\mu\text{F cm}^{-2}$)	Electrochemical surface area (ECSA) (m^2g^{-1})	Turnover Frequency (TOF) (s^{-1})
NiFe@CNT	2.3	28.4	0.9

NiFe(2,2'-bpy)@CNT	5.5	67.9	1.67
NiFe(2,2'-bpy) ₂ @CNT	8.1	100	1.86
NiFe(2,2'-bpy) ₃ @CNT	9.9	122.2	1.27
NiFe(2,2'-bpy) ₄ @CNT	6.1	75.3	0.17
NiFe(2,2'-bpy) ₅ @CNT	5.8	71.6	0.011
NiFe(2,2'-bpy) ₆ @CNT	2.8	34.6	0.007

Note:

$$C_{dl} = I/v;$$

$$ECSA = C_{dl}/(C_s * m);$$

$$TOF = jS/(4nF)$$

(where I is the capacitive current (mA cm^{-2}) and v is the scan rate (mV s^{-1}); C_s is the specific capacitance of a planar surface (0.04 mF cm^{-2}), and m is the loading amount of catalysts on the surface of glassy carbon electrode in this work: ca. 2 g/m^2 ; j (mA cm^{-2}) is the measured current density at a given overpotential $\eta = 300 \text{ mV}$, S (0.1963 cm^2) is the surface area of GCE electrode, n is the total mole of metal atoms on the electrode, F (96485 C mol^{-1}) is Faraday constant, the number of 4 means that 4 electrons transfer per O_2 molecule.)

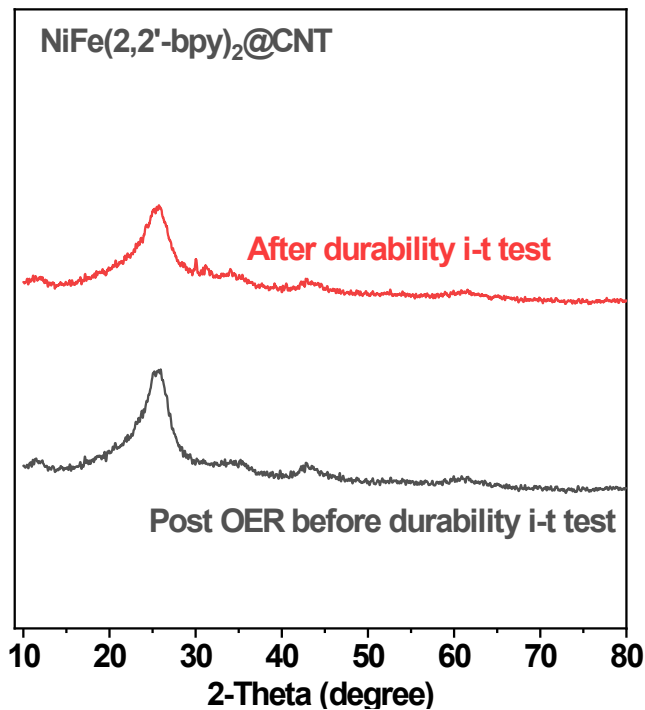
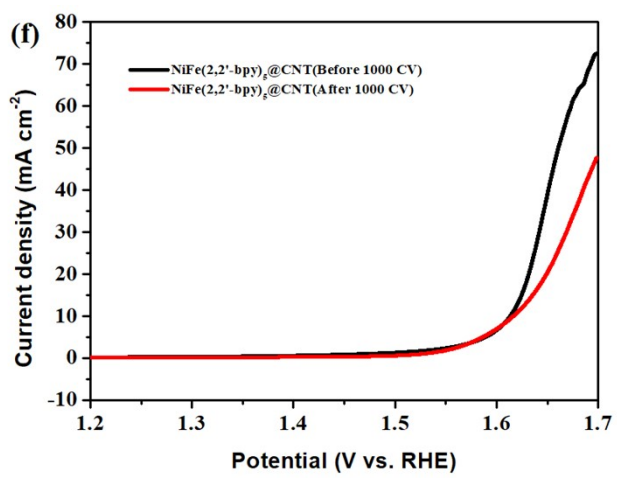
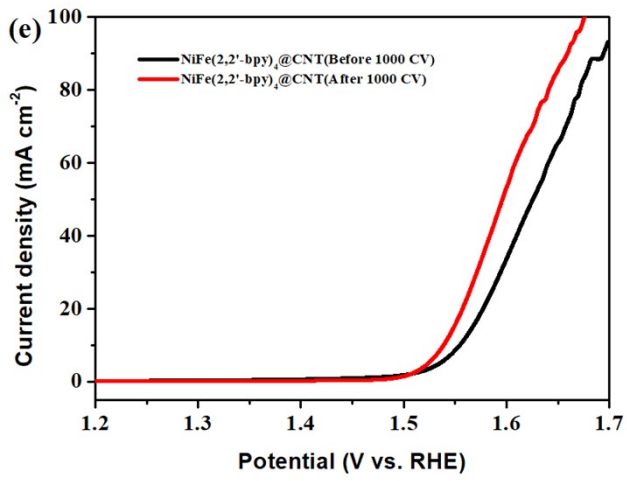
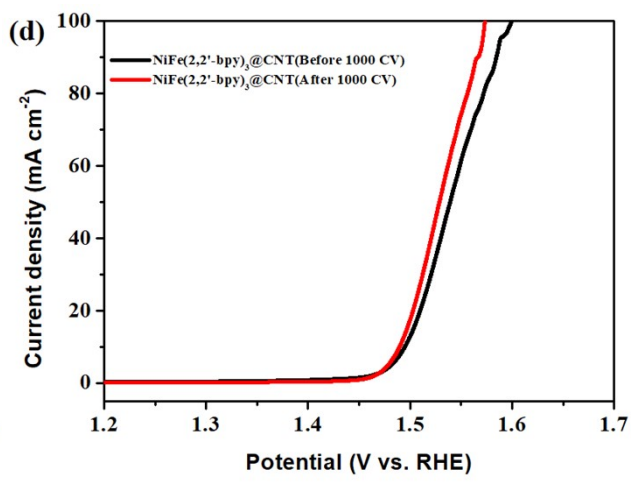
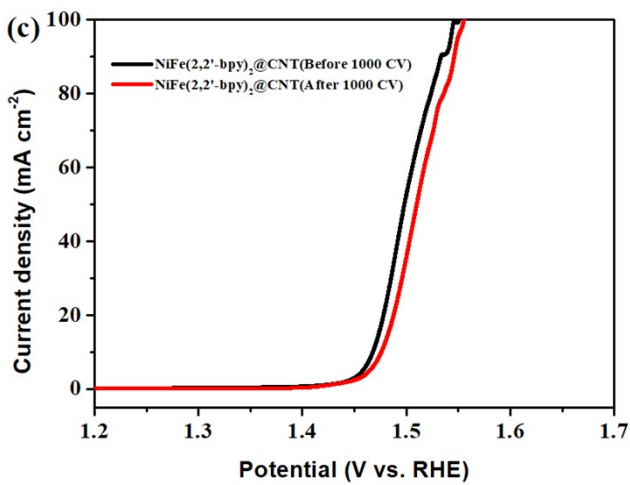
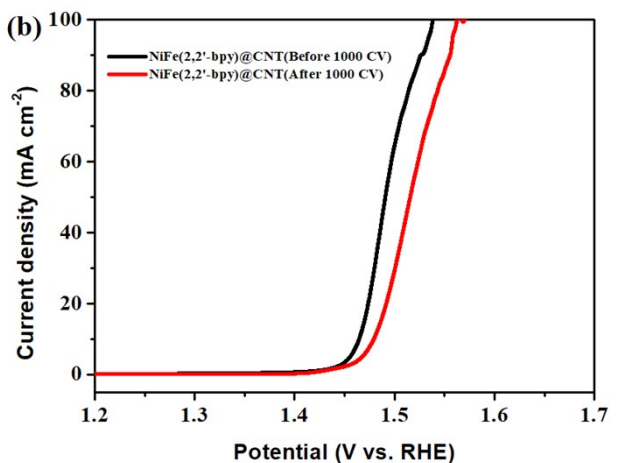
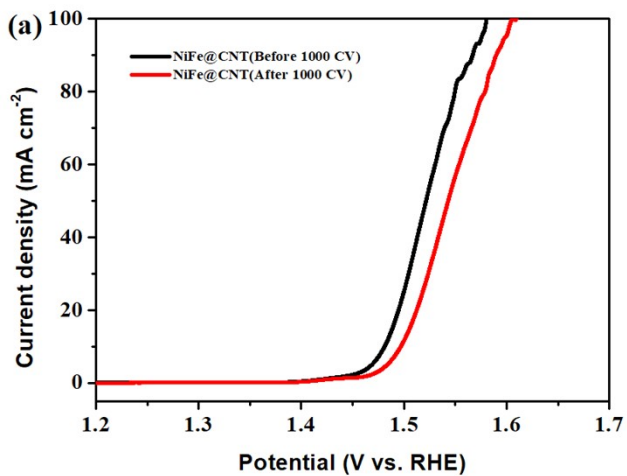


Figure S8 XRD of the best-performing sample, NiFe(2,2'-bpy)₂@CNT before and after long-term durability i-t test



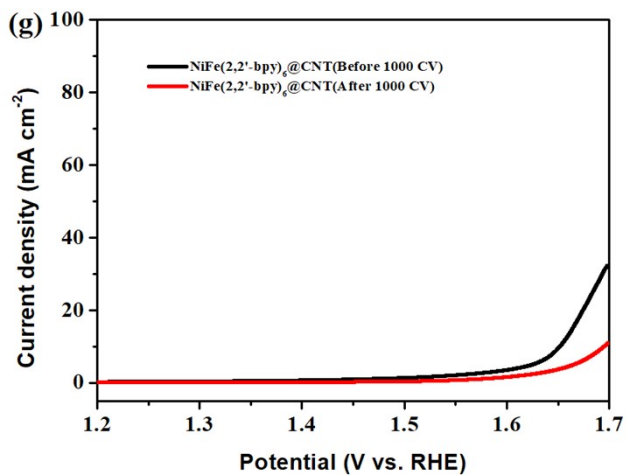


Figure S9 LSV curves of NiFe($2,2'$ -bpy)_n@CNT before and after 1000 CV cycles at 1.2–1.7 V

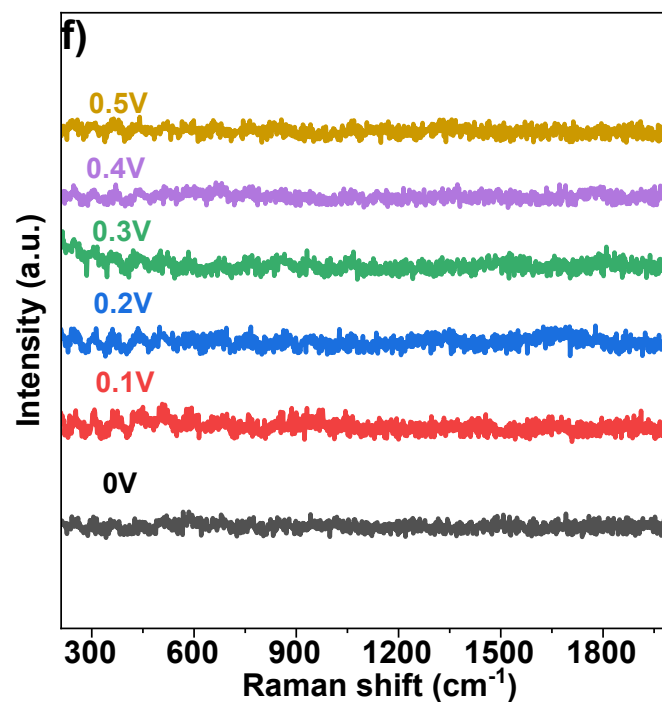
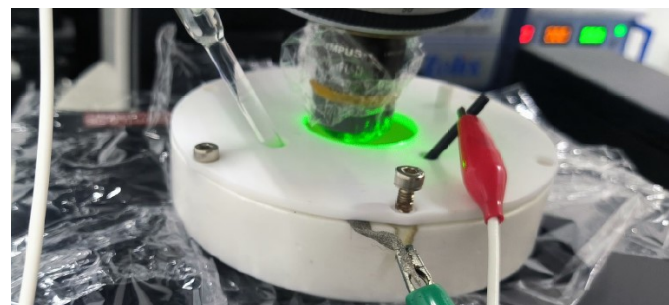


Figure S10 In Situ Raman Spectroscopy measurement of NiFe($2,2'$ -bpy)₂ at different applied potential.

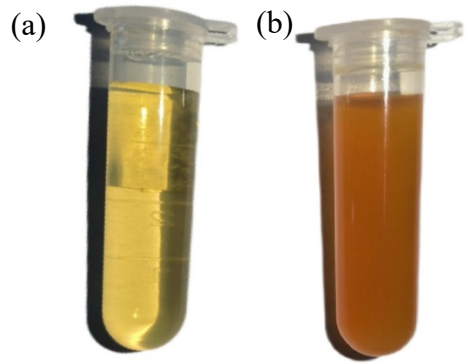
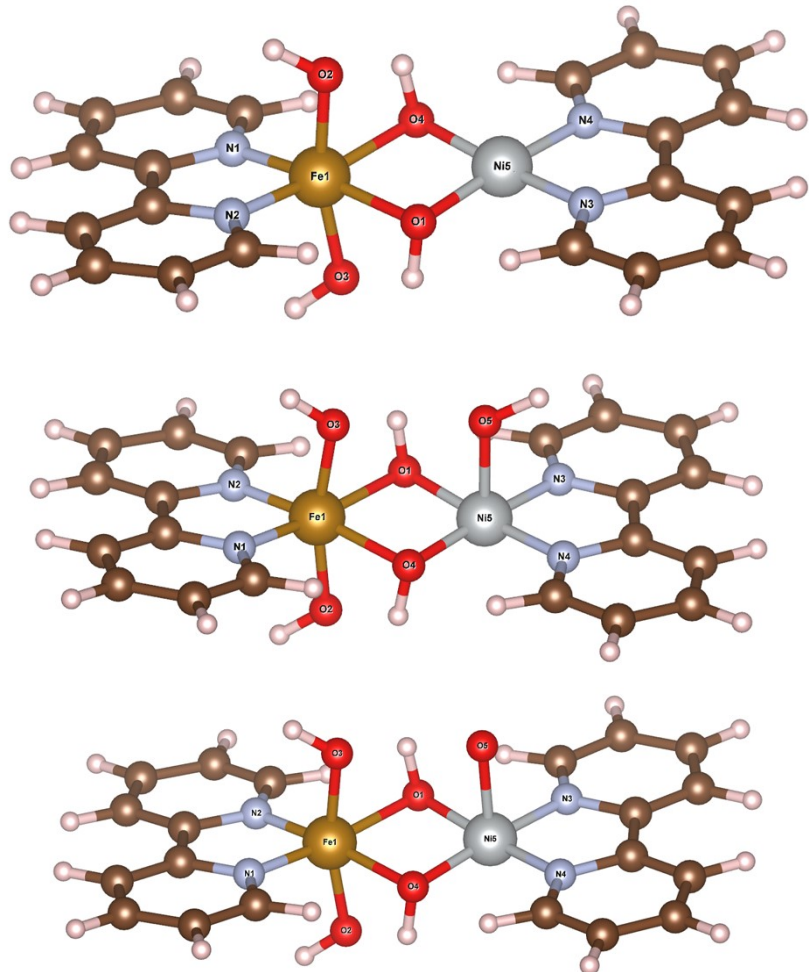
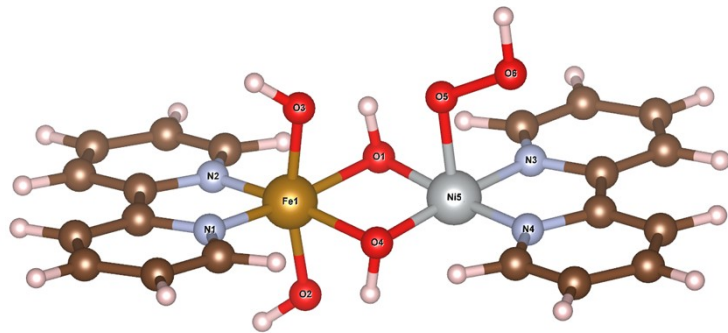
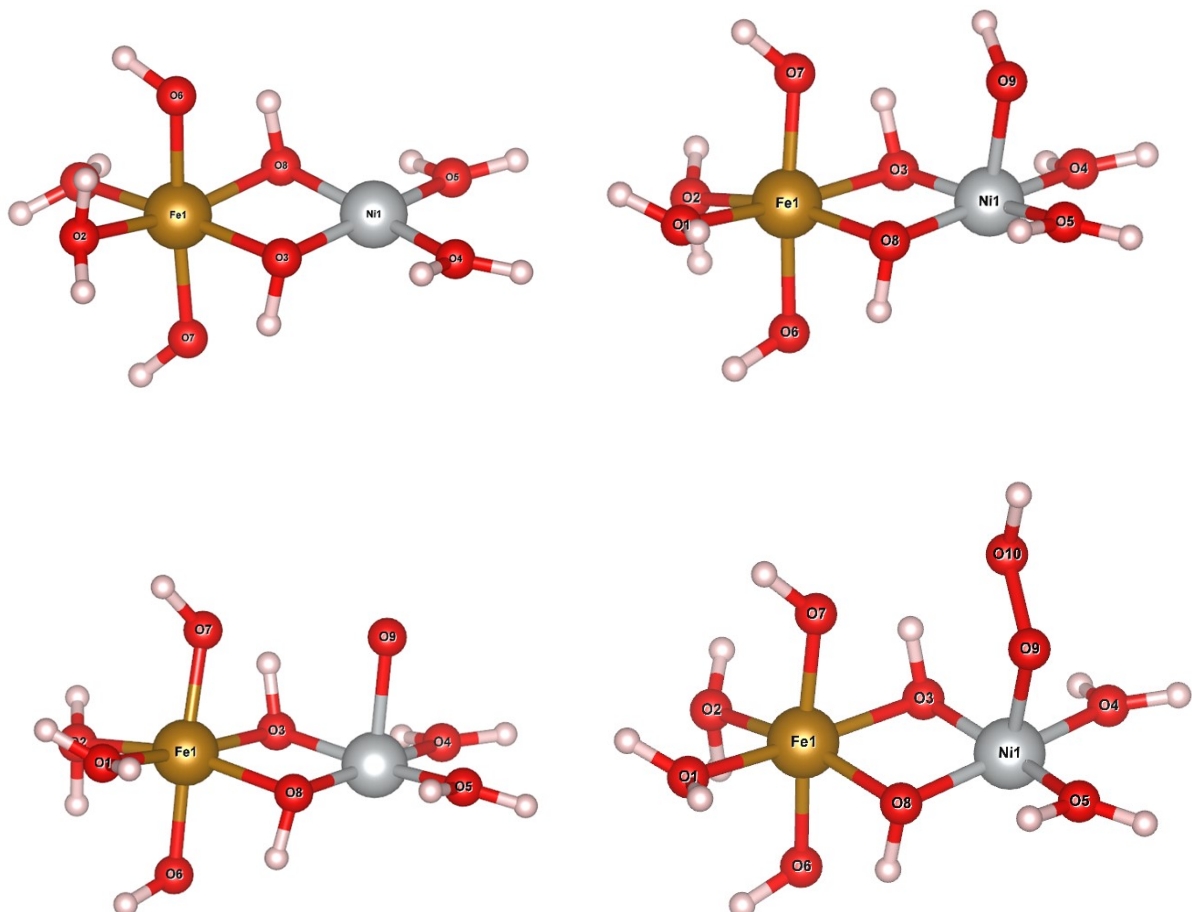


Figure S11 (a) Depicts the outcome of $\text{NiFe}(\text{2,2-bpy})_2$ drops in water; (b) shows the result of $\text{NiFe}(\text{2,2-bpy})_2$ drops in a 1M KOH solution.

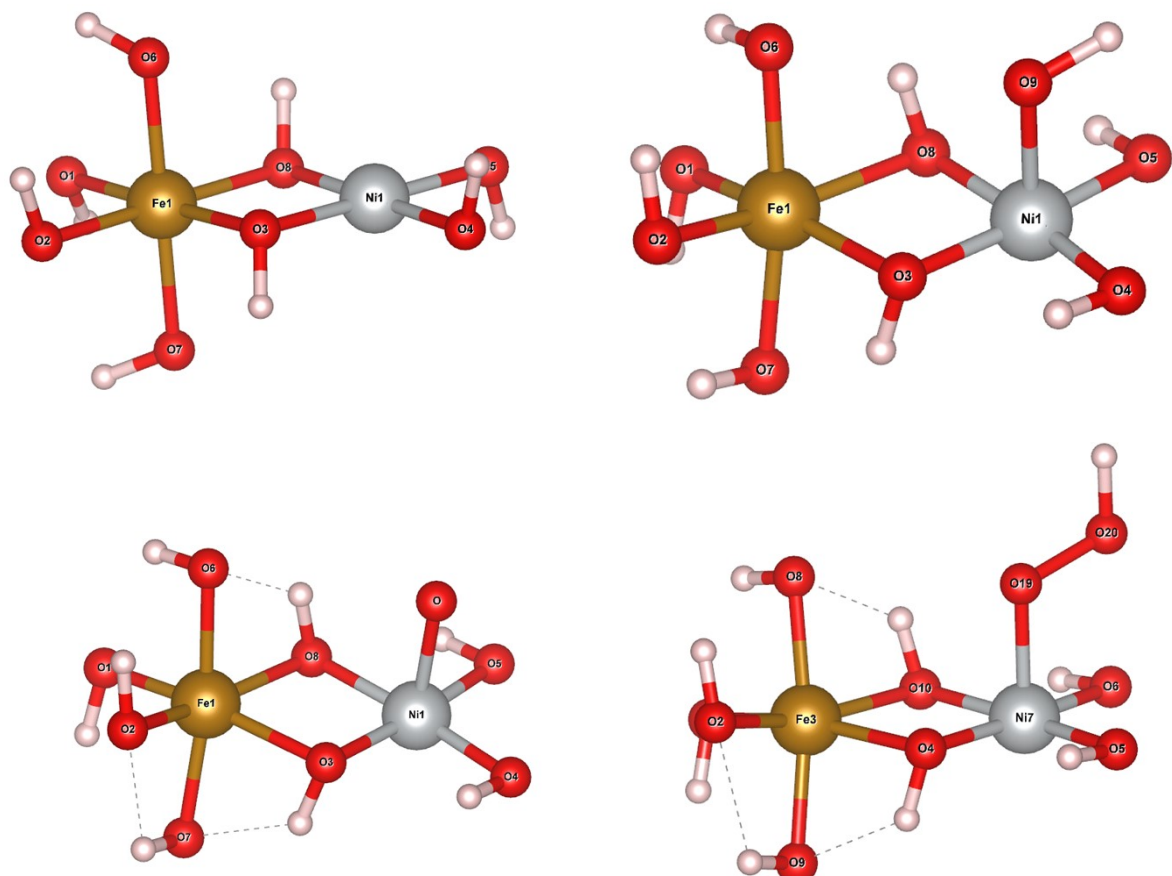




(a) Catalytic intermediates *, *OH, *O, *OOH (* = $\text{NiFe}(\text{OH})_4(2,2'\text{-bpy})_2$)



(b) Catalytic intermediates *, *OH, *O, *OOH (* = $\text{NiFe}(\text{OH})_4(\text{H}_2\text{O})_4$)



(c) Catalytic intermediates *, *OH, *O, *OOH (* = NiFe(OH)₈)

Figure S12 The molecular models used for DFT calculation described in the Text

Table S4 Comparison of OER performance of catalysts in 1 M KOH

Materials	10 mA cm ⁻² overpotential mV	Tafel slope mV dec ⁻¹	Substrate	TOF value s ⁻¹	Stability (10 mA/cm ²)	Reference
NiFe(2,2'-bpy) ₂ @CNT	240	42.4	GCE ^a	1.86	15 h	This work
a-CoPSe	223mV @ 100 mA/cm ²	32	NF	35.7	100 h at 100 mA/cm ²	1
Fe ²⁺ -NiFe LDH	249	40.3	CFP	0.09	15h	2
NiCo _{2-x} Fe _x O ₄ NBs	274	42	CFP	0.016	25h	3
30% Ce-NiFe-LDH	242	34	GCE	0.011	24h	4
NiFe LDH-UF	254	32	GCE	0.06	12h	5
HG-NiFe	310	39	GCE	0.53	5.5h	6
Fe-doped-(Ni-MOFs)/FeOOH	210 mV @ 15 mA/cm ²	50	NF	56.8	120 h	7
FeOOH@NiFe LDH(0.2 M)	252mV @ 100 mA/cm ²	51.49	NF	4.61	100 h at 100 mA/cm ²	8

Ni-MIL-53-Fc	297 mV @ 50 mA/cm ²	60.2	CFP	1.25	-	9
NiFe LDH nanomesh	268 mV @ 50 mA/cm ²	30	GCE	1.49	48h	10
FeNi LDH sheet/FeNi	130	39	NF	0.072	10h	11
NiFeV LDHs	192	42	NF	0.04	18h	12
Ni _{0.67} Fe _{0.33} /C	210	35	GCE	0.3	28h at 40 mA/cm ²	13
CoFe LDH HNC	238	42	NF	0.05	50 h	14

^aGCE = Glassy Carbon Electrode; NF = Nickel foam; CFP = Carbon Fiber Paper

- (1) Shi, Y.; Zhou, S. L.; Liu, J. X.; Zhang, X.; Yin, J.; Zhan, T. R.; Yang, Y.; Li, G. J.; Lai, J. P.; Wang, L., An Integrated Amorphous Cobalt Phosphoselenide Electrocatalyst with High Mass Activity Boosts Alkaline Overall Water Splitting. *Appl. Catal. B Environ.* **2024**, *341*, 123326.
- (2) Cai, Z.; Zhou, D. J.; Wang, M. Y.; Bak, S. M.; Wu, Y. S.; Wu, Z. S.; Tian, Y.; Xiong, X. Y.; Li, Y. P.; Liu, W.; Siahrostami, S.; Kuang, Y.; Yang, X. Q.; Duan, H. H.; Feng, Z. X.; Wang, H. L.; Sun, X. M., Introducing Fe²⁺ into Nickel-Iron Layered Double Hydroxide: Local Structure Modulated Water Oxidation Activity. *Angew. Chem., Int. Ed.* **2018**, *57*, 9392-9396.
- (3) Huang, Y.; Zhang, S. L.; Lu, X. F.; Wu, Z. P.; Luan, D. Y.; Lou, X. W., Trimetallic Spinel NiCo_{2-x}Fe_xO₄ Nanoboxes for Highly Efficient Electrocatalytic Oxygen Evolution. *Angew. Chem., Int. Ed.* **2021**, *60*, 11841-11846.
- (4) Xu, H. J.; Shan, C. F.; Wu, X. X.; Sun, M. Z.; Huang, B. L.; Tang, Y.; Yan, C. H., Fabrication of Layered Double Hydroxide Microcapsules Mediated by Cerium Doping in Metal-Organic Frameworks for Boosting Water Splitting. *Energy Environ. Sci.* **2020**, *13*, 2949-2956.
- (5) Zhao, Y. F.; Zhang, X.; Jia, X. D.; Waterhouse, G. I. N.; Shi, R.; Zhang, X. R.; Zhan, F.; Tao, Y.; Wu, L. Z.; Tung, C. H.; O'Hare, D.; Zhang, T. R., Sub-3 nm Ultrafine Monolayer Layered Double Hydroxide Nanosheets for Electrochemical Water Oxidation. *Adv. Energy Mater.* **2018**, *8*, 1703585.
- (6) Wang, J.; Gan, L. Y.; Zhang, W. Y.; Peng, Y. C.; Yu, H.; Yan, Q. Y.; Xia, X. H.; Wang, X., In Situ Formation of Molecular Ni-Fe Active Sites on Heteroatom-Doped Graphene as a Heterogeneous Electrocatalyst toward Oxygen Evolution. *Sci. Adv.* **2018**, *4*, eaap7970.
- (7) Li, C. F.; Xie, L. J.; Zhao, J. W.; Gu, L. F.; Tang, H. B.; Zheng, L. R.; Li, G. R., Interfacial Fe-O-Ni-O-Fe Bonding Regulates the Active Ni Sites of Ni-Mofs Via Iron Doping and Decorating with FeOOH for Super-Efficient Oxygen Evolution. *Angew. Chem., Int. Ed.* **2022**, *61*, e202116934.
- (8) Li, Y.; Wu, Y. Y.; Yuan, M. K.; Hao, H. R.; Lv, Z.; Xu, L. L.; Wei, B., Operando Spectroscopies Unveil Interfacial FeOOH Induced Highly Reactive β-Ni(Fe)OOH for Efficient Oxygen Evolution. *Appl. Catal., B* **2022**, *318*, 121825.
- (9) Xu, Z. Z.; Tao, Y.; Sun, Z. D.; Bi, P. Y.; Zhong, X.; Liao, J. J.; Hao, D. C.; Yang, L. C.; Xu, L.; Luo, M. B.; Pan, K. C.; Gao, Z., Ligand-Engineered Ni-Based Metal-Organic Frameworks for Electrochemical Oxygen Evolution Reaction. *Chem. Eng. J.* **2023**, *478*, 147418.
- (10) Xie, J. F.; Xin, J. P.; Wang, R. X.; Zhang, X. D.; Lei, F. C.; Qu, H. C.; Hao, P.; Cui, G. W.; Tang, B.; Xie, Y., Sub-3 nm Pores in Two-Dimensional Nanomesh Promoting the Generation of Electroactive Phase for Robust Water Oxidation. *Nano Energy* **2018**, *53*, 74-82.
- (11) Xiang, Q.; Li, F.; Chen, W. L.; Ma, Y. L.; Wu, Y.; Gu, X.; Qin, Y.; Tao, P.; Song, C. Y.; Shang, W.; Zhu, H.; Deng, T.; Wu, J. B., In Situ Vertical Growth of Fe-Ni Layered Double-Hydroxide Arrays on Fe-Ni Alloy Foil: Interfacial Layer Enhanced Electrocatalyst with Small Overpotential for Oxygen Evolution Reaction. *ACS Energy Lett.* **2018**, *3*, 2357-2365.
- (12) Li, P. S.; Duan, X. X.; Kuang, Y.; Li, Y. P.; Zhang, G. X.; Liu, W.; Sun, X. M., Tuning Electronic Structure of NiFe

Layered Double Hydroxides with Vanadium Doping toward High Efficient Electrocatalytic Water Oxidation. *Adv. Energy Mater.* **2018**, *8*, 1703341.

(13) Yin, S. M.; Tu, W. G.; Sheng, Y.; Du, Y. H.; Kraft, M.; Borgna, A.; Xu, R., A Highly Efficient Oxygen Evolution Catalyst Consisting of Interconnected Nickel-Iron-Layered Double Hydroxide and Carbon Nanodomains. *Adv. Mater.* **2018**, *30*, 1705106.

(14) Ni, Y. M.; Shi, D. R.; Mao, B. G.; Wang, S. H.; Wang, Y.; Ahmad, A.; Sun, J. L.; Song, F.; Cao, M. H.; Hu, C. W., Under-Coordinated Cofe Layered Double Hydroxide Nanocages Derived from Nanoconfined Hydrolysis of Bimetal Organic Compounds for Efficient Electrocatalytic Water Oxidation. *Small* **2023**, *19*, 2302556.